



---

## Determination of the elasto-plastic behaviour of the various phases of a bulk cement paste by means of micro-indentation tests and FE simulation

Dame KEINDE<sup>1</sup>, Fabrice BERNARD<sup>2\*</sup>, Siham KAMALI-BERNARD<sup>2</sup>,  
Marilyne CORNEN<sup>3</sup>

<sup>1</sup>Ecole Supérieure Polytechnique de Dakar, Civil Engineering Department, Dakar, Sénégal

<sup>2</sup>University of Rennes, INSA Rennes, Laboratory of Civil Engineering and Mechanical Engineering, Rennes, France

<sup>3</sup>University of Rennes, INSA Rennes, UMR CNRS 6226 Institut des Sciences Chimiques de Rennes, Rennes, France

\* Corresponding author: [dame.keinde@esp.sn](mailto:dame.keinde@esp.sn)

---

**Abstract** The purpose of this paper is to determine the elasto-plastic behavior of various phases of a Hardened Cement Paste. A coupled experimental-numerical investigation is presented. A large campaign of microindentation tests has been first performed. These experiments are led on concrete samples. The statistical analysis of the experimental results based on the deconvolution method as well as micro-analyses with Scanning Electron Microscopy has allowed to distinguish five different groups of phases, namely LowDensity C-S-H, High Density C-S-H, Portlandite CH, unhydrated particles and sand grains, as well as their relative proportions. Mean force-indentation depth curves characteristics of each phase are identified.

The simulation of these indentation tests is then performed by the Finite Element Method. A nonassociated plasticity model based on a Drucker-Prager plastic potential and the Yield function proposed by Lubliner and modified by Lee and Fenves is chosen to represent the behaviour of the various phases of the cementitious material. An inverse determination of the parameters of these two function governing the plastic behaviour, based on the demonstration of their influence on the load-indentation depth, is developed.

The results may be used by researchers involved in hierarchical multi-scale modelling of cement-based materials.

**Keywords** Indentation experiment, deconvolution, statistical analysis, cement-based materials, FE simulation, nonassociated plasticity, inverse analysis

---

### 1. Introduction

Most of the properties and durability aspects of concrete are linked to hardened cement paste characteristics. It is therefore of the most importance to understand the hydrated cement paste basic structure to better understand the concrete physico-chemical properties. Clinker consists of four main components:  $C_3S$ ,  $C_2S$ ,  $C_3S$ , and  $C_4AF$ . Cement paste has a very complex microstructure which varies in function of the cement composition, time and hydration conditions. To make things simpler, the main components of the microstructure are the hydrated calcium Silicates (C-S-H), the portlandite (CH), the calcium trisulfoaluminate also called ettringite (noted AFt), the monosulfoaluminate (AFm). Moreover, anhydrous cement grains and micro-porosity are found.

The C-S-H are the main hydration products. These are porous components with amorphous and colloidal structures and a variable chemical composition. The portlandite CH often occurs in the shape of massive crystals, but is also mixed with C-S-H at the micromillimeter scale. The portlandite CH and the cement clinker can be considered as non-porous solid components.



Different works have been carried out in the last few decades to study the solid components of the Hardened Cement Paste and their elastic properties. Indeed, these last years, the tremendous increase of computational capabilities has largely favoured the development of numerical modellings based on a realistic and multi-scale description of cementitious materials. The intent is to assist the material developer by providing a rational approach to material development and concurrently assist the structural designer by providing an integrated analysis tool that incorporates fundamental material behaviour (among the most recent publications: [1-15], including some of the co-authors of this work [16-26]).

It is now clear that any realistic attempt to accomplish such an objective should be based on a precise determination of the properties of each individual components of the cementitious materials.

Nano-indentation is undoubtedly a meaningful experimental technique that enables researchers to characterize local mechanical properties, especially with the development of new techniques and instruments at the micro- and nano-scales. Thus a considerable effort, in the past recent years, has been devoted to such studies on various heterogeneous materials. In early years, micro-indentation tests have allowed to estimate first the properties of the bulk cement paste [27,28], and then the elastic modulus and strength of the Interfacial Transition zone [29-31]. Nano-indentation techniques have then been developed to obtain submicro-scale mechanical properties and more particularly those of the individual components of the Hardened Cement Paste. This technique has enabled materials scientists to go deeper in the knowledge of cementitious materials microstructure. The existence of two kinds of C-S-H, with their relative proportions, has been put into evidence [32,33]. Thus, at a microscopic scale, observing

C-S-H in a hydrated cement paste reveals two different textures. The first one called HD (high density) C-S-H or inner C-S-H, has a dense aspect and is found inside the initial cement grain and the other one, called LD (low density) C-S-H or outer C-S-H has an aspect that is less dense, more fibrous and more dispersed, as illustrated in Figure 1.

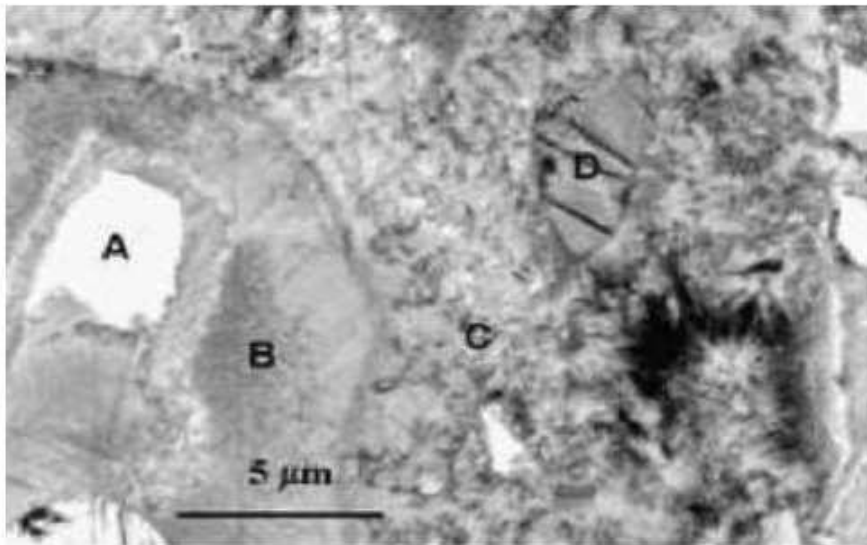


Figure 1: Backscattered electron image of a cement paste: A grain of anhydrous cement; B HD C-S-H ; C LD C-S-H ; D monosulfoaluminate ou AFm [Diam 2006]

The terms “inner C-S-H” and “outer C-S-H” come from Scrivener’s research work [34], whereas Jennings [35], when performing nitrogen absorption tests, identified two types of C.S.H porosity accessibility and termed them as HD C-S-H and LD C-S-H.

Based on these first referenced experimental works, statistical analyses of nano-indentation tests were proposed and carried out to determine the nano-mechanical behaviour of the components of Hardened Cement Pastes. The original studies were devoted to CEM I type cement in normal or elevated temperature conditions [36], and then extended to supplementary cementitious materials [37,38], ultrahigh performance concrete [39], and also recycled aggregates concrete [40].

Despite some questionings about the relevance of the methodology [41] which was in debate [42,43], numerous results have been obtained and have enabled researchers to determine firstly the elastic properties of the components of Hardened Cement Paste, see for example the recent publication of Lin et al. [44].

Simulations of the nano-indentation tests allowed to extent the determination of the mechanical properties of the indented materials. Thus various inverse analyses strategies have been established in recent years to study viscoelastic [45] and even plastic or cracking behaviour [46-51]. In these recent studies, plasticity models with few parameters to determine have been considered. The use of a more complex nonassociated plasticity based model for the various components of a Hardened Cement Paste, as the one used in the present paper, has not been discussed yet.

Furthermore, up to now, experimental campaigns have been carried out on pure phases or on cement paste and rarely on composites with the aggregates and therefore with the Interfacial Transition Zone, at the noticeable exception of the works presented before [29-31,40]. However, the mixture with aggregates and the appearance of this transition zone modify the bulk paste [22,23,52].

Thus, the aim of this paper is to develop an approach making it possible to study the matrix inside the cementitious composite. This determination is obviously highly important for the cement matrix characterization. The methodology can be applied for sustainable questions. The present paper first introduces the material and methods and then examines the material results. Finally, it exploits the results by using statistical methods. Then, a FE simulation of the test is presented, as well a sensitivity analysis on each of the model parameters to identify. The procedure has enabled us to find how these parameters influence the force-depth curve and finally allowed their determination. The results may be used as input data for the multi-scale modeling of the mechanical behaviour of cementitious materials. The objective for such modelling strategies is to assist structural engineers by providing accurate constitutive laws and also simulation tools able to use these laws, as well as to propose a rational approach for the materials development.

## 2. Material and methods

The work presented in this paper is part of a project devoted to the characterization and the modeling of cementitious composites at both micro and meso-scales. Thus the material used in this study is a concrete prepared with a CEM I type cement and a water-to-cement ratio of 0.5, 0/4 sand, 6/10 and 10/20 aggregates. The mass composition was as follows: 0/4 sand = 710 kg / m<sup>3</sup>; 6/10 aggregates = 365 kg / m<sup>3</sup>; 10/20 aggregates = 725 kg / m<sup>3</sup>; CEM I cement = 400 kg/m<sup>3</sup>.

A 7 x 7 x 28 cm parallelepipedic sample was made up and vibrated to eliminate air bubbles (figure 2). After 24 hours, the sample was withdrawn from its mold and was immediately put in a damp room for maturation. After ten days, a diamond saw was used to cut out the sample in order to obtain small 1.5 x 1.5 x 2 cm parallelepipedic samples. These ones were put in a dessicator. The samples surfaces were then polished by using several abrasive cloths. The sizes of the diamond particles varied from 6 μm to 0.25 mm. Thus, in this study, the focus was on low hydration degrees. It should, however, be noted that the experimental methodology set up does not depend on maturation time.



Figure 2: Parallelepipedal specimen (a) and storage condition in desiccator



As previously explained, nano- or micro-indentation techniques have been used for some years to assess the elastic properties of cement materials or pure components (see also [53]).

In this new research work, an effort was made to be located at a scale higher than in [36] in order to identify homogenized properties of a concrete matrix. If the choice was made upon this mesoscale, it was because the aim was to consider the matrix modification by adding a granular skeleton. The tests were performed at room temperature, the measuring device used was a Micro scratch tester, manufactured by CSM (Figure 3). The used indenter had a spherical shape with a diameter equal to 10 μm. On the sample, 99 indentations were made on an area of 250 x 240 μm in the cement matrix located near aggregates, the area having been chosen randomly (Figure 3). Spacing among the centers of gravity of indents was fixed at 25 μm into a direction and at 30 μm into the perpendicular direction. The load used for all the indents was fixed at 25 mN.



Figure 3: Nano/micro-indenter used in the study: micro-scratch tester manufactured by CSM

At the indentation place, the surface was about to be distorted in a way which reflected the mechanical properties of the indented material. The elastic modulus and the hardness could be calculated in function of the maximum load and the maximum penetration. The method to be used was that of Olivier and Pharr [54]. This method describes the upper part of the unloading curve by the following law:

$$F = F_{\max} \left( \frac{h - h_p}{h_{\max} - h_p} \right)^m \quad (1)$$

Where  $F$  is the force,  $F_{\max}$  is the maximum force applied,  $h$  is the indentation depth;  $h_p$  is the indentation depth after unloading,  $h_{\max}$  is the maximum indentation depth at  $F_{\max}$ ;  $m$  is a constant determined by using a least squares method and is function of indenter geometry.

An example of load-indentation depth curve achieved in the present work is presented in Figure 4.

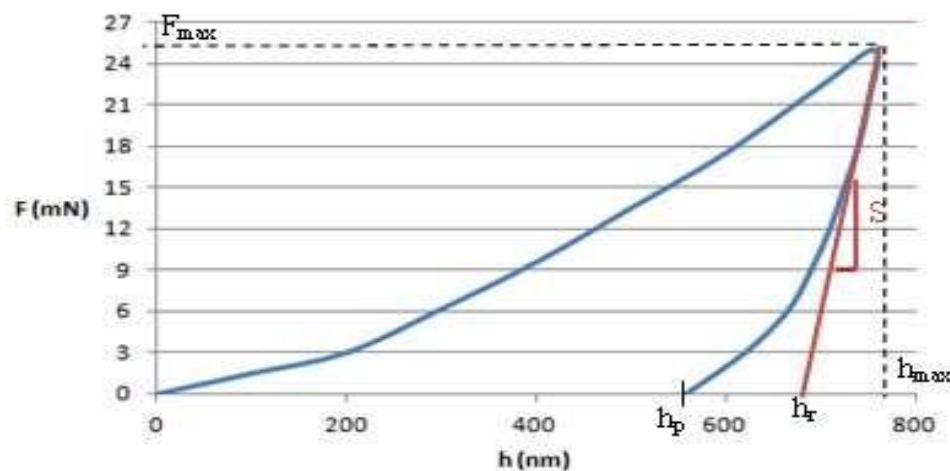


Figure 4: Analysis of the micro-indentation test. Achievement of contact stiffness and depth

The different parameters of equation 1 are defined as follows.

Contact stiffness  $S$  is given by the curve tangent at the maximum force contact:

$$S = \left( \frac{dF}{dh} \right)_{\max} \quad -1 = m \quad (2)$$

$F_{\max}(h_{\max} - h_p)$  Prolonging this tangent allows to define  $h_r$ :

$$h_r = h_{\max} - \frac{F_{\max}}{S} \quad (3)$$

Contact depth  $h_c$  is then determined by

$$h_c = h_{\max} - \varepsilon(h_{\max} - h_r) \quad (4)$$

Where  $\varepsilon$  depends on exponent  $m$  and thus on the indenter shape. For a spherical indenter,  $\varepsilon = 1$ .

Hardness  $H_{IT}$  is identified from the maximum load,  $F_{\max}$ , of the projected contact surface  $A_p$  at the contact depth  $h_c$ ,  $A_p$  is function of the contact depth  $h_c$  and is determined by calibration of the indenter.

$$H_{IT} = \frac{F_{\max}}{A_p(h_c)} \quad (5)$$

The reduced modulus  $E_r$  is given by

$$E_r = \frac{F_{\max}}{A_p(h_c)} \quad (6)$$

This reduced modulus is function of the Young's modulus and the Poisson's coefficient of the indented material (unknown) and the indenter material (known). Also, without a hypothesis on one of the unknown parameters (Young's modulus and Poisson coefficient of indented material), it is not possible to decorrelate them by using this technique:

$$\frac{1}{E_r} = \frac{1 - \nu_s^2}{E_{IT}} + \frac{1 - \nu_i^2}{E_i} \quad (7)$$

Where  $E_i$  and  $\nu_i$  were respectively the elastic modulus and Poisson's coefficient of the indenter and  $\nu_s$ ,

Poisson's coefficient of the sample. In the present research study:  $\nu_i = 0.07$  and  $E_i = 1141$  GPa. Most of the experimental results were presented hereafter in terms of reduced modulus of the indented material. If it is not the case, it was assumed in a first approach that  $\nu_s = 0.24$ , a value commonly allowed for the mortar.

Conventionally, indentation methods were applied to homogenous materials. As already said, Constantinides and Ulm [36] extended this technique to materials made up of several components but also at different scales. To apply this technique called indentation grid technique, a very large series of indentation tests had to be carried out on a surface grid. Then each indentation test was considered as a statistical event, and the mechanical properties extracted from the indentation test, namely the elastic modulus ( $E$ ) and the hardness ( $H$ ) were considered as random variables. The data were then analyzed by deconvolution of frequencies densities. It was assumed that the distribution of the mechanical properties  $x = E$  or  $H$  of each component  $j$  was very well approximated by the normal (or Gaussian) distribution:

$$P_j(x) = \frac{1}{\sqrt{2\pi S_j^2}} \exp\left(-\frac{(x - \mu_j)^2}{2S_j^2}\right) \quad (8)$$

Where  $\mu$  is the arithmetic average of all the  $N_j$ -values for each component, while the standard deviation  $s_j^2$  is the dispersion of these values:

$$\mu_j = \frac{1}{N_j} \sum_{k=1}^{N_j} x_k \quad \text{and} \quad S_j^2 = \frac{1}{N_j - 1} \sum_{k=1}^{N_j} (x_k - \mu_j)^2 \quad (9)$$

$n=1$  corresponds to the homogenous material case, in the case of several components which all had a normal distribution and which did not interact one with the others, the total frequency distribution complied with the probability density function:

$$p(x) = \sum_{j=1}^n f_j p_j(x) \quad (10)$$

Where  $f_j = N_j/N$  is the surface fraction occupied by component  $j$



$$\sum_{j=1}^n f_j = 1 \tag{11}$$

The problem thus defined includes  $3n-1$  unknown values, that is to say 3 unknown values per component ( $\mu_j, s_j, f_j$ ), reduced by the compatibility condition (previous equation). The responses distribution was obtained in the form of discrete values  $P_i$ . Consequently the unknown values could be determined by minimizing the error defined as follows:

$$\sum_{i=1}^m \frac{(p_i - p(x_i))^2}{m} \tag{12}$$

(12)

Where,  $p_i$  is the experimental value of the frequency density,  $p(x_i) = \sum_{j=1}^n f_j p_j(x_i)$  is the theoretical value of the probability density function at point  $x_i$ , and  $m$  the number of intervals chosen to build the histogram.

### 3. Analyzing the micro-indentation results

Figure 5 shows the distribution of the 99 indents performed on the matrix. The indented area was visualized by using an optical Microscope. Figure 5 shows the cement matrix surrounded by aggregates on its contour and highlights the indented area limited by a black line. A number is provided for each indent during the micro-indentation test.

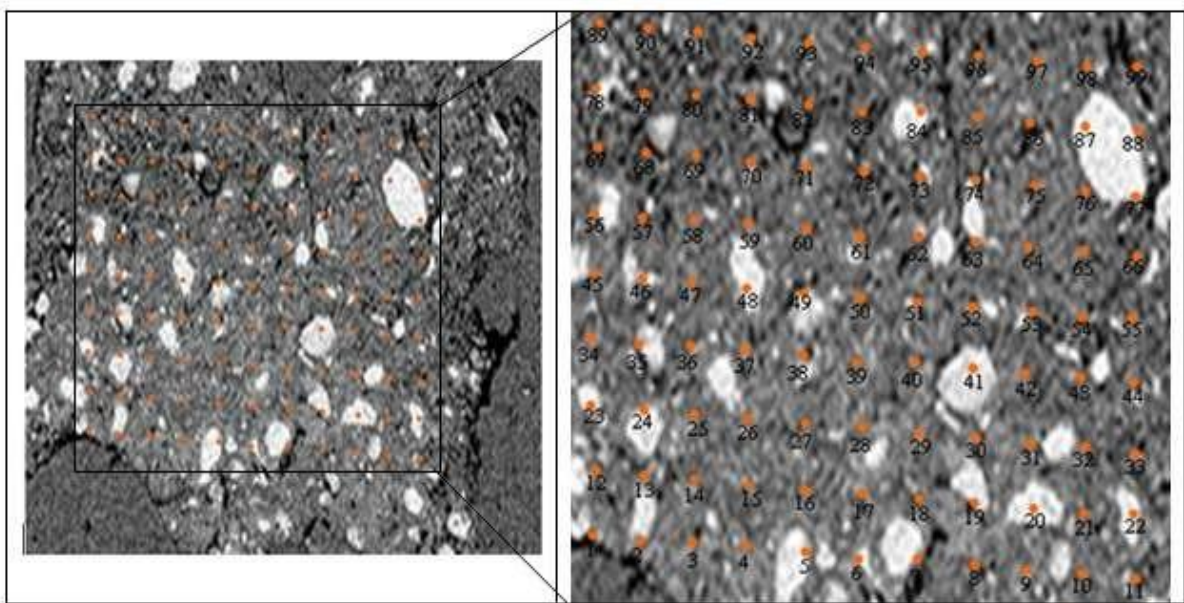


Figure 5: Test area and numbering of the indents

To show the different components of the indented area, images by Scanning Electron Microscopy were made. Figure 6 shows the indented area too. The sand grains are grey, the anhydrous grains are small white particles, the hydration products (C-S-H mainly) are coloured in light grey and the gaps and other pores are in black. Figures 7 to 10 present micro-analyses performed on each of the matrix components.

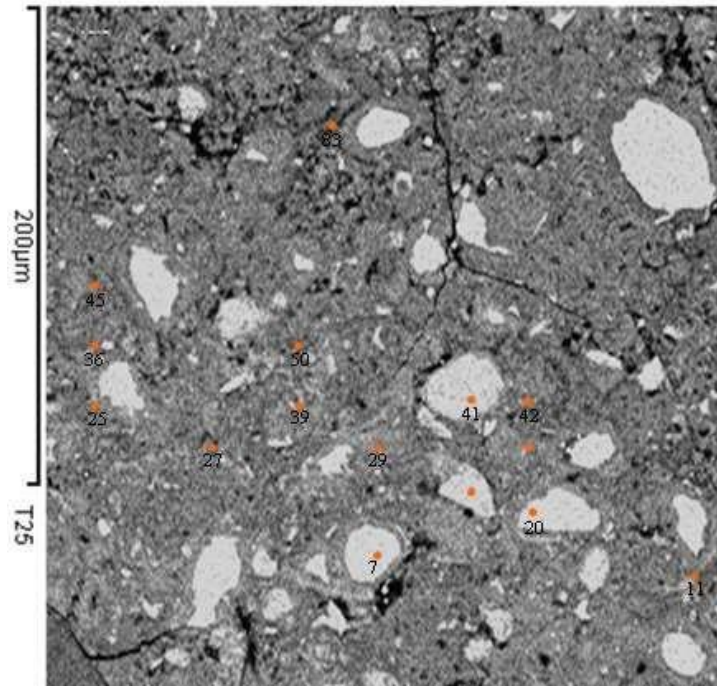


Figure 6: Zoom on the indented area

Élément	%Masse	%Atomique
OK	50.85	69.98
AlK	0.88	0.72
SiK	11.90	9.33
CaK	36.37	19.98
Totaux	100.00	

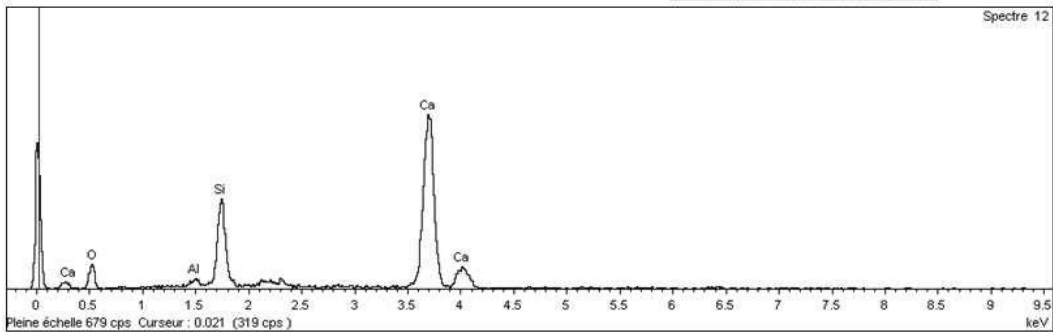
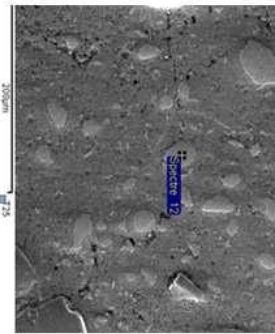


Figure 7: Micro-analyses performed on some matrix components

Elément	%Masse	%Atomique
OK	53.55	71.95
MgK	0.69	0.61
AlK	1.19	0.95
SiK	10.96	8.39
SK	1.81	1.22
CaK	30.74	16.49
FeK	1.06	0.41
Totaux	100.00	

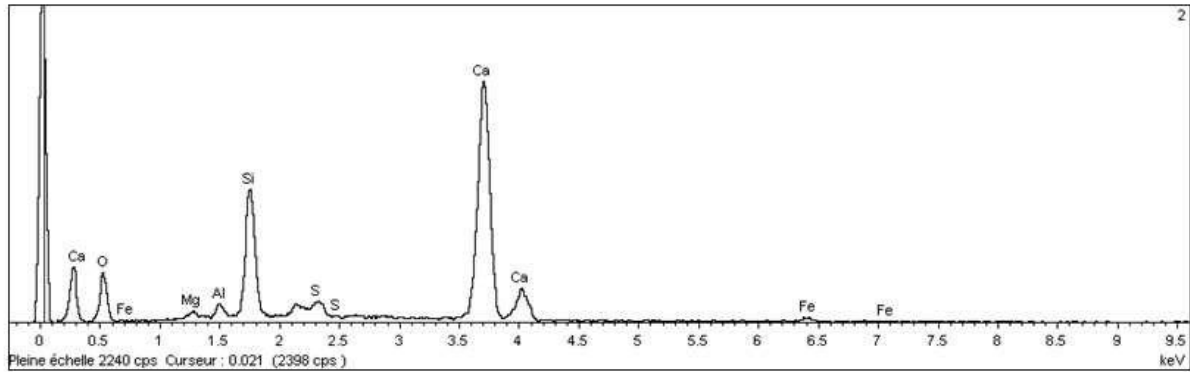
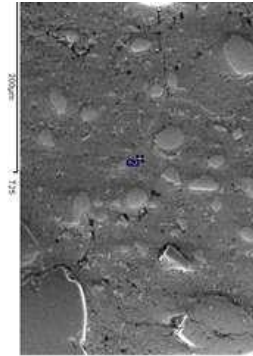


Figure 8: Micro-analyses performed on some matrix components

Elément	%Masse	%Atomique
OK	57.87	75.47
AlK	0.92	0.71
SiK	10.64	7.90
CaK	30.57	15.91
Totaux	100.00	

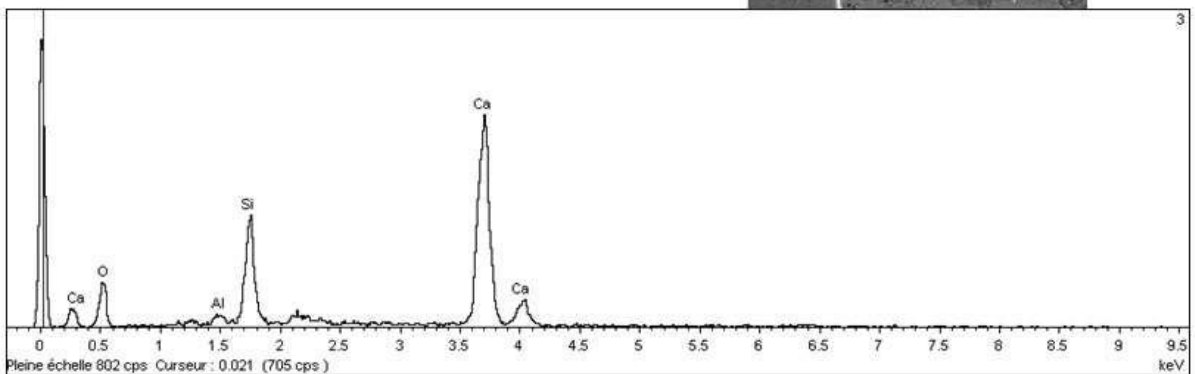
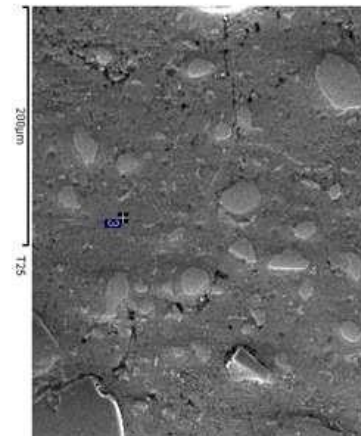


Figure 9: Micro-analyses performed on some matrix components

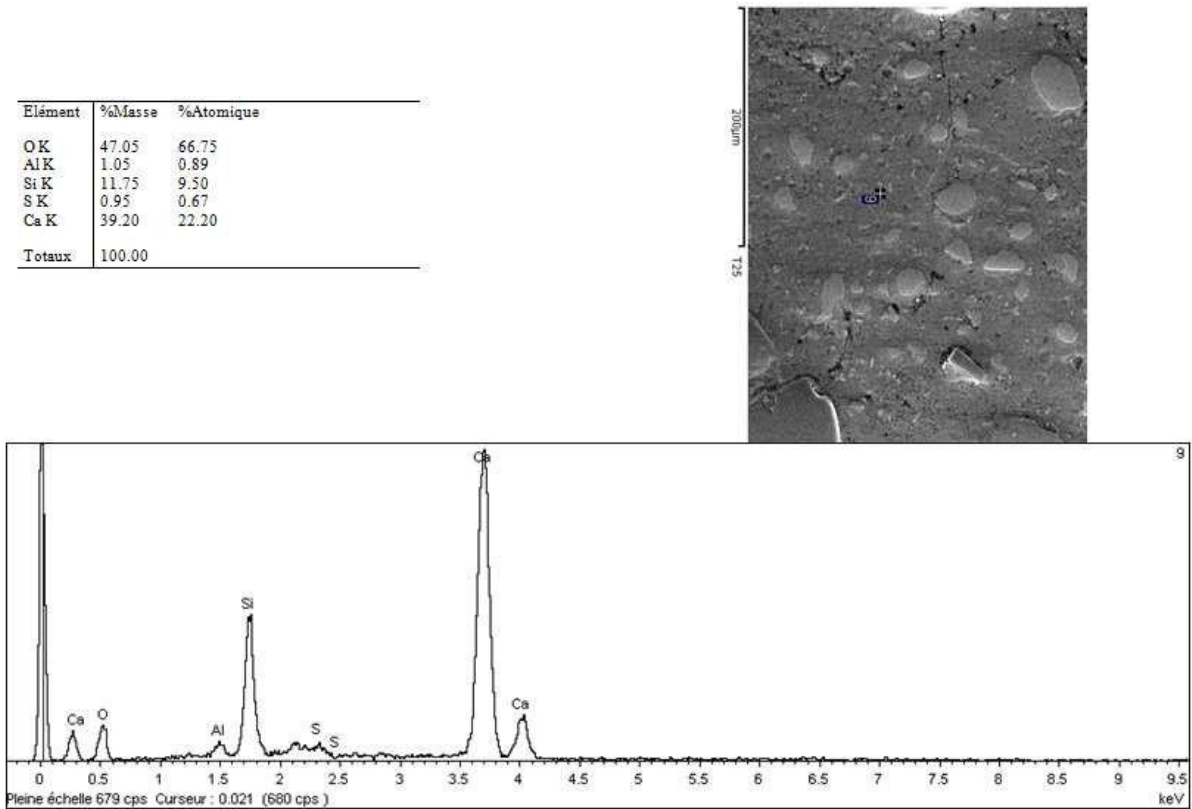
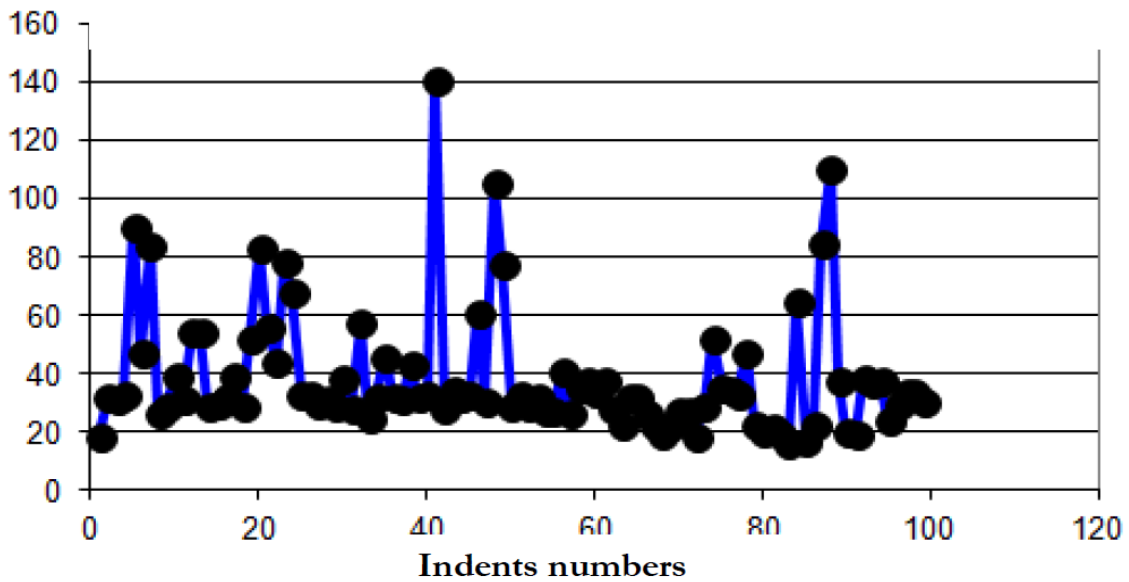


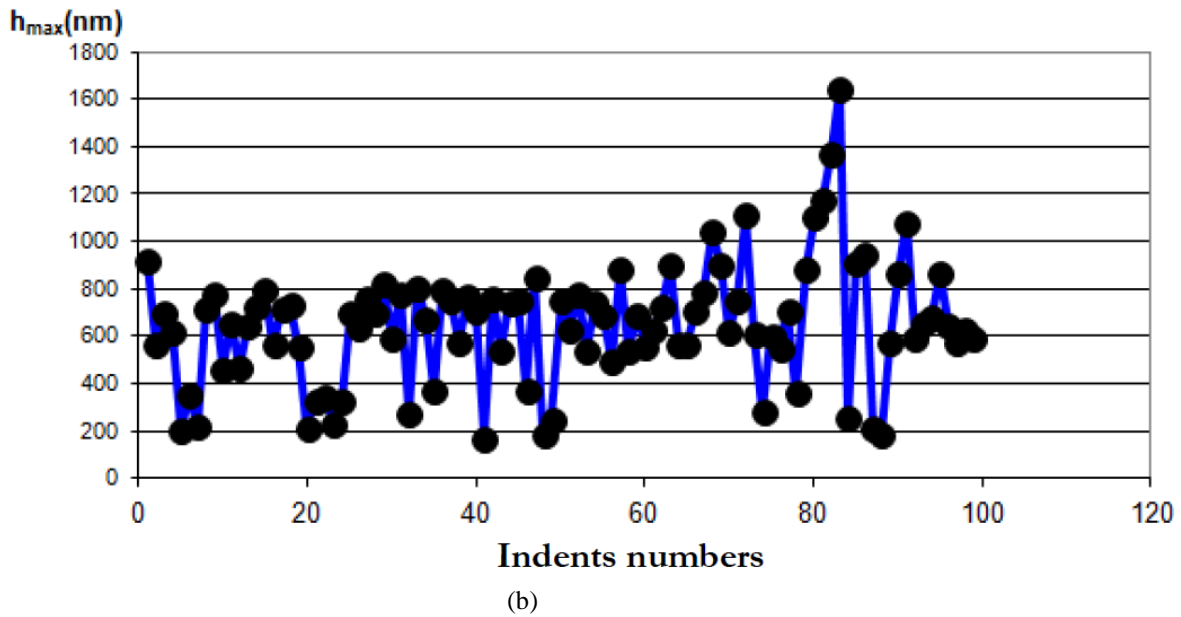
Figure 10: Micro-analyses performed on some matrix components

Figure 11 presents the evolution of the reduced elastic modulus  $E_r$  (in GPa) and of the maximum depth  $h_{max}$  (in nm) in function of the indented position of the sample used. The large variations of the values thus highlighted are a consequence of the heterogeneity of the material and of the position of the indented point according to the aggregate, around which is a transition aureole of higher porosity than the rest of the matrix. This figure, expectedly, also shows that a high Young modulus is translated into a low indentation depth and reciprocally.

$E_r$  (GPa)



(a)



(b)  
 Figure 11: Micro-indentation results. Modulus of elasticity E (a) and maximum depth (b) in function of the number of indent

**4. Exploiting the results by the statistical method.**

By applying the statistical method, 5 groups of experimental values are obtained (Figure 12).

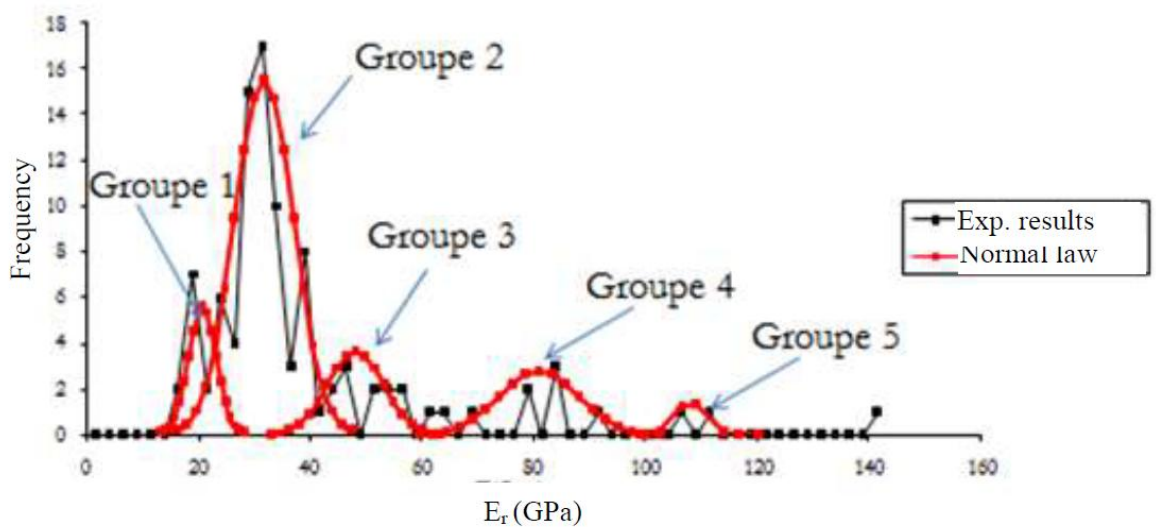


Figure 12: Experimental micro-indentation results. Distribution of reduced elastic modulus

The histogram first peak area called Group 1 belongs to interval [16-27 GPa] and the mean value of the reduced Young ‘s modulus is equal to  $21.1 \pm 2.17$  GPa. The values within this interval are associated with areas where the indentation response is very likely dominated by the LD C-S-H. Using nanoindentation on a w/c=0.5 hardened white cement paste, Constantinides and Ulm [36] found that the LD C-S-H reduced elastic modulus is equal to  $18.2 \pm 4.2$  GPa. Acker [55] gives a value of  $20 \pm 2$  GPa.

The estimated volume fraction of this component is here equal to 19.19%.

The histogram second peak area called Group 2 belongs to interval [27-39] GPa and the mean value of the reduced elastic modulus is equal to  $31.4 \pm 3.6$  GPa. The values within this interval are associated with areas where the indentation response is very likely dominated by the HD C-S-H. Constantinides and Ulm [36] found

that the reduced elastic modulus of this component is equal to  $29.4 \pm 2.4$  GPa. Acker [55] gives a value of  $31 \pm 4$  GPa.

The estimated volume fraction of the HD C-S-H is here equal to 55.55%.

The histogram third peak area called Group 3 belongs to interval [39-60] GPa and the mean value of the reduced elastic modulus is equal to  $47.99 \pm 5$  GPa. The values within this interval are associated with areas where the indentation response is likely dominated by Porthandite CH. Constantinides and Ulm [36] found that the reduced elastic modulus of this component is equal to  $40.3 \pm 4$  GPa. Acker [55] gives a value of  $36 \pm 4$  GPa. The estimated volume fraction of the CH is here equal to 12.12%.

The histogram fourth and fifth peak area called Group 4 and Group 5 belongs to interval [60-141] GPa and the average values of the reduced elastic modulus are respectively equal to  $81 \pm 5.2$  and  $107 \pm 3.4$ . The values within this interval are associated with areas where the indentation response is respectively dominated by sand and clinker. The two components are not always discernible by simple observation. The combined volume fraction of the two components is equal to 13.13%.

Some modulation, however, needs to be considered when showing these groups accurately. Indeed, given the load level, the indenter may possibly have touched two groups simultaneously.

It is also worth noting that HD C-S-H are here the dominant component in the cement matrix. They represent 74% of the C-S-H volume. This established fact is in contradiction with the results previously achieved on the aggregateless paste. Constantinides and Ulm [36] when studying a pure paste, found that the dominant component is the LD C-S-H and that the latter represented 65% of the volume of the C-S-H.

A possible explanation could be linked to the presence of the sand grains and aggregates which cause the appearance of the high porosity transition aureole and, as a result, the decrease of the cement matrix porosity. So the w/c ratio for a matrix without aggregate is greater than that of the hardened cement paste with aggregates. And the LD C-S-H or outer C-S-H are known to be formed in the pores full of water during hydration. Besides, the paste studied by [36] was completely hydrated without the presence of clinker while, in the present study, the observation of the cement matrix studied using SEM shows the significant presence of anhydrous grains, which means that the hydration is not complete.

To indirectly validate the results coming from the deconvolution technique, it would be interesting to simulate the micro-indentation test. This simulation could be carried on until the determination of inelastic properties of each component, which could not be assessed by an experimental test. Each group would be represented by an experimental diagram characterized by an elastic modulus close to the mean value of the group. The experimental diagrams representative of each group are represented in the Figure 13.

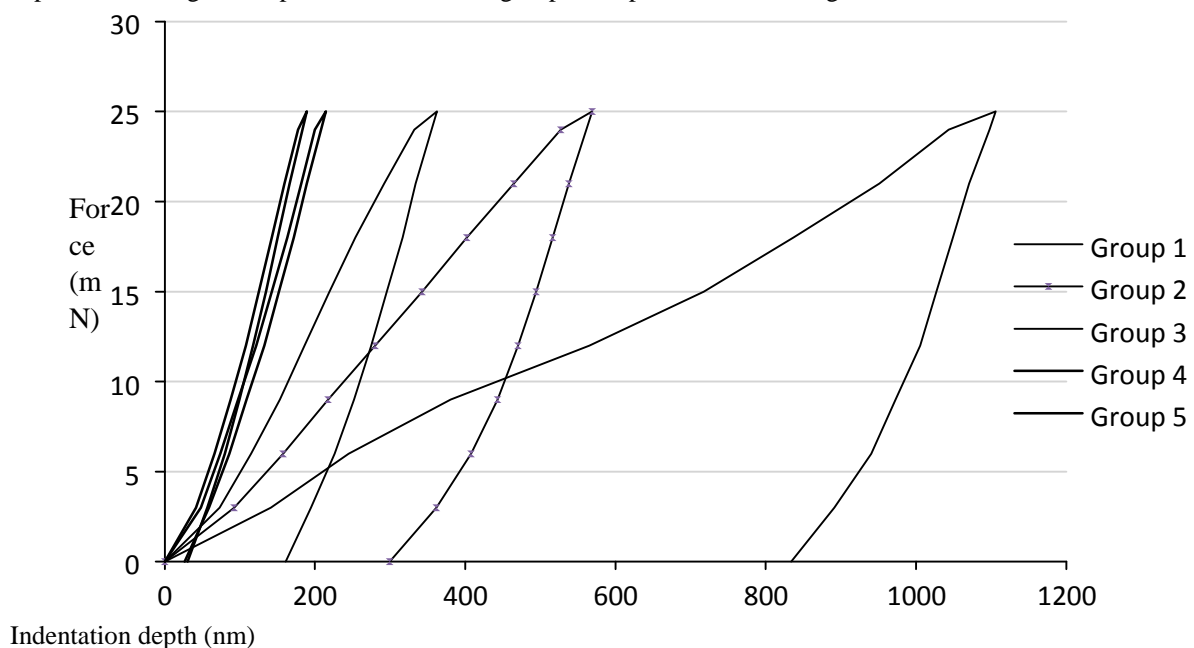


Figure 13: Mean force-indentation depth curve for the whole groups



The analysis of the experimental diagrams representative of the different groups makes it possible to note that for the same maximum load of 25 mN, the maximum indentation depth for LD C-S-H (first group) is twice as big as the second group (HD C-S-H) and three times as for the third group. The residual distortion of the first group follows the same trend. Besides, the plastic area, delimited by the horizontal axis, the loading diagram and the unload diagram, is greater for groups 1 and 2 and is almost equal to zero for groups 4 and 5. Consequently interesting information can be drawn on the different components of the cement matrix:

- LD C-S-H are the component that can most be distorted and have a large plastic distortion. This behaviour is due to a high porosity as this phase is formed in pores full of water and has a fibrous texture [55]. According to Ghabezloo [56] their porosity is equal to 0.37. As a result, it can be said to have an elastoplastic behaviour.
- HD C-S-H are a component that can be distorted, with plastic distortion inferior to that of LD C-S-H. According to Ghabezloo [56] their porosity is equal to 0.24. Their behaviour can also be qualified as elastoplastic.
- The CH is also an elastoplastic component that can little be distorted compared with the first two groups. The area, limited by the horizontal axis, the load diagram and the unloading diagram is seen to be lower than those of the LD C-S-H and HD C-S-H.
- As far as the sand grains and clinker are concerned, they exhibit an almost purely elastic behaviour for this range of effort applied as their residual distortion is low and the area limited by the horizontal axis, the load diagram and the unloading curve is almost equal to zero. Nevertheless, their behaviour is considered as remaining elastoplastic.

These considerations can be used as guiding principles in the choice of the behaviour law to be used for each component.

## 5. Finite Element simulation of the micro-indentation test to identify the parameters of the constitutive law for the various phases of the Hardened Cement Paste in mortar

### 5.1 Constitutive law for the mechanical behaviour of the various phases of HCP and main parameters to identify

The experimental force-depth curves put into evidence nonlinearities in the response of the indented phases. Concrete behaviour is the result of local distortions at a microscopic level. As aggregates, in ordinary concrete, can be considered as being, in no way, out the elastic field of their behaviour, the concrete composite elastoplastic behaviour is governed by that of the cement matrix, and so, by its different components and their association, namely the C-S-H, portlandite (CH) and, possibly, the unhydrated clinker. As previously said, analyzing the representative experimental curves of the different cement matrix phases showed that the latter have an elastoplastic behaviour. To describe this behaviour, it is necessary to, in addition to the elastic field, determine the main characteristics of the nonlinear behaviour of the different cement matrix phases.

An elastoplastic law can also be justified by the nanogranular nature of hydrates [36,57]

In this work, the plastic behaviour of the various phases is first characterized by the Yield function of Lubliner et al. [58] modified by Lee and Fenves [59]. This function is defined as follows:

$$F = \frac{1}{1 - \alpha} (q - 3\alpha p + \beta(\epsilon^{pl})\hat{\sigma}_{\max} + \gamma\hat{\sigma}_{\max}) - \sigma_c(\epsilon^{pl}) \quad (13)$$

In which:

-  $\gamma = \frac{3(1-K)}{3K-1}$  with K the ratio of the second stress invariant on the tensile meridian to that of the compressive meridian,

- q the deviatoric equivalent stress,  $q = \sqrt{\frac{3}{2}(\boldsymbol{\sigma} + p) : (\boldsymbol{\sigma} + p)}$ ,

- p the hydrostatic pressure stress  $p = -\frac{1}{3}\text{trace}(\boldsymbol{\sigma})$ ,

-  $\hat{\sigma}_{\max}$  the maximum principal stress,



$$\beta(\varepsilon^{pl}) = \frac{\sigma_c(\varepsilon_c^{pl})}{\sigma_t(\varepsilon_t^{pl})} (1 - \alpha) + (1 + \alpha)$$
 with  $\sigma_c(\varepsilon_c^{pl})$  and  $\sigma_t(\varepsilon_t^{pl})$  respectively the compressive and tensile stress cohesions and  $\alpha = \frac{(f_b/f_{c0})-1}{2(f_b/f_{c0})-1}$  where  $f_b$  is the equibiaxial compressive yield stress and  $f_{c0}$  the uniaxial compressive yield stress.

This Yield function is often used in damaged plasticity models for cementitious materials. It is written here in the stress plane and not in the effective stress plane as damage and microcracking are not supposed to be generated in the phases indented by a spherical indenter, as in this study, as contrary to Berkovich indenter for example.

Then, the plastic model considered in this work introduces a non-associated plastic flow potential, different thus from the yield function. The Drucker-Prager model is used here, with its elliptical shape,

$$G = \sqrt{(R_c - eR_t \tan \Psi)^2 + q^2} - p \tan \Psi \quad (14) \text{ for the definition of this potential, given by:}$$

Where:

- $R_t$  and  $R_c$  are the uniaxial tensile and compressive strengths of the considered phase respectively,
- $\Psi$  is the dilation angle measured in the p-q plane at high confining pressure, -  $e$  is an eccentricity of the plastic potential surface.

As explained in previous sections, the micro-indentation test makes it possible to extract directly (without any particular inverse method) two parameters of the material namely Young's modulus (by means of a hypothesis on Poisson's coefficient) and hardness. Moreover, given the difficulty linked to calculating a slope on an experimental curve, it was decided not to use the values previously determined and to consider Young's modulus and Poisson's coefficient as parameters to be identified. The purpose of the following of the paper is thus to determine the parameters of each phase starting from the microindentation test by using a numerical approach coupled to an inverse method. The inverse method principle consists in iteratively minimizing the gap between the simulation result and the experimental measurement. The parametric identification problem is the most used inverse problem in indentation.

In summary, the whole parameters to identify are:

- For the elastic part of the behaviour:  $E$  the Young's modulus of the considered phase,  $\nu$  the Poisson coefficient of the considered phase;
- $R_c$  and  $R_t$ , respectively the compressive and tensile strengths of the considered phase;
- For the plastic part of the behaviour: the parameters of the Drucker-Prager plastic flow potential, namely the dilation angle  $\Psi$  and the eccentricity  $e$ , and those of the Yield function, that is to say: the ratio between the equibiaxial and the uniaxial compressive yield stresses, and  $K$  the ratio of the second stress invariant on the tensile meridian to that of the compressive meridian.

As a whole, 8 variable parameters defining the mechanical behaviour of the various phases have to be identified. It is worth noting that the research works carried out so far to characterize the properties of cement paste phases have been achieved in the elastic field.

## 5.2 Simulation of the micro-indentation test

### 5.2.1 Main hypotheses of the simulation

The simulation of the micro-indentation test has been performed using the FE software package ABAQUS [60]. Axisymmetric conditions are assumed. The spherical indenter has been described by a rigid surface; its diameter is 10  $\mu\text{m}$ . Each phase is simulated alone imposing thus that the material is homogenous. Figure 14 shows a cross-section of the mesh with the half-sphere and a homogenous considered phase. Figure 15 presents a 3D view of the mesh used for this simulation obtained with an axisymmetric revolution. A finer mesh has been assigned to the area located directly under the indentation point and an unrefined mesh has been attributed far away from the indenter (figure 14). That made it possible to achieve more accuracy and, at the same time, reduce the calculation time duration.

For surfaces in contact, a contact pair approach is considered.



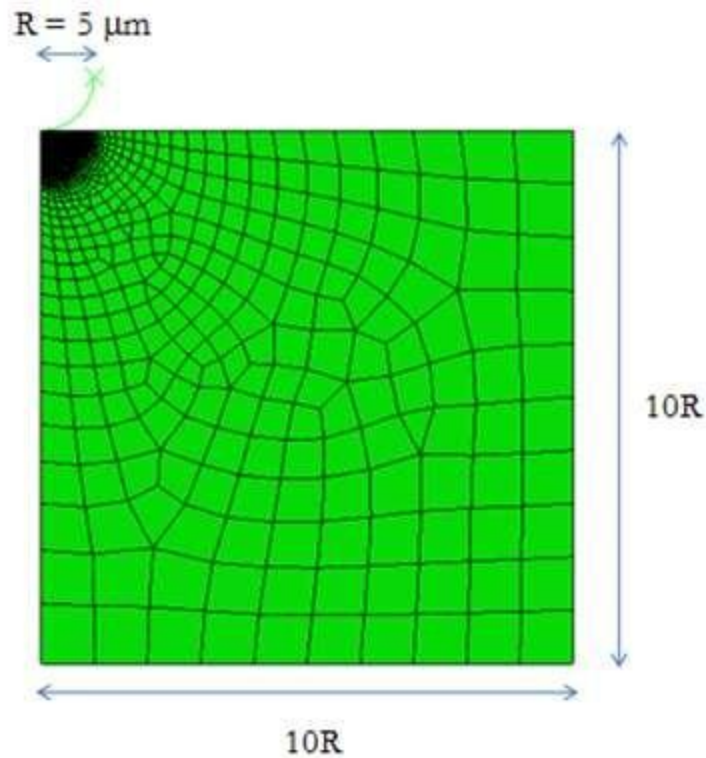


Figure 14: Cross section of the mesh used to simulate the micro-indentation test

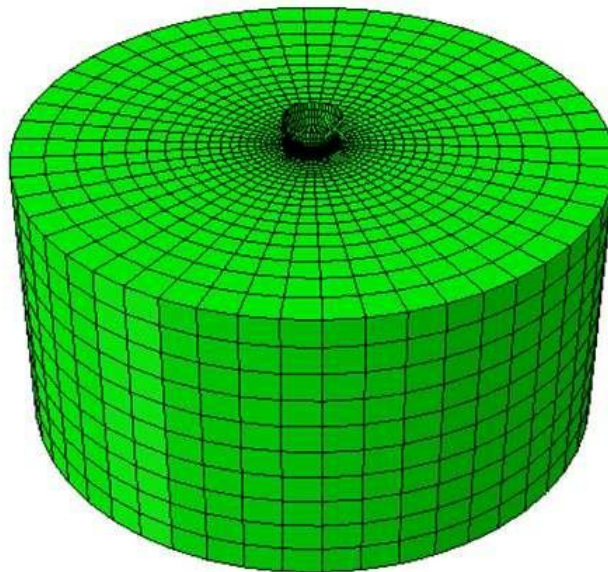


Figure 15. 3D view of the mesh used to simulate the micro-indentation test

More particularly, the small-sliding, surface-to-surface formulation has been chosen. This formulation requires the definition of slave and master surfaces. In the case of the use of rigid surface, this one is the master surface. Furthermore, a Coulomb friction to define the tangential behaviour of the contact is considered.

The test simulation has been performed in imposed displacement conditions whereas an imposed force has been used during the experimental test. The imposed displacement is set equal to the maximum displacement deduced from the representative experimental force-depth curve. An increasing displacement is thus applied on the node of the rigid sphere in contact with the indentation point of the mesh until this maximum displacement value is reached. Then the displacement is continuously decreased until a zero value. The reaction force and the depth of the indentation point are recorded, which enables one to plot the force-depth curve.

### 5.2.2 Sensitivity analysis on the friction coefficient

As previously explained, a Coulomb model to describe the contact between indenter and indented surface is used. The tangential contact behaviour is governed by the value of the friction coefficient. In this part of the work, the evolution of the indentation force-depth curve is studied for various values of the friction coefficient. The set of materials parameters used is arbitrarily fixed at  $E=48$  GPa,  $\nu=0.32$ ,  $R_c=50$  MPa and  $R_t=3.6$  MPa. They correspond to that of the Portlandite phase. Moreover, to define yield function and plastic flow potential, the parameters considered by default for cementitious materials in Abaqus user's manual [60] or in literature are used:  $\Psi=35^\circ$  [61],  $K=0.66$ ,  $\alpha=1.16$  and  $e=0$ .

Figure 16 presents the results obtained for this first sensitivity analysis. It can be seen that the friction coefficient between the material and the indenter has an influence only on the maximum force and affects neither the residual strain nor the unloading curve slope. Yet, the results seem less influenced by the friction coefficient beyond a value equal to 0.6. Sarris and Constantinides [62] have also investigated this point and have found that beyond 0.25 there was not much influence. Later, the friction coefficient will be considered equal 0.6.

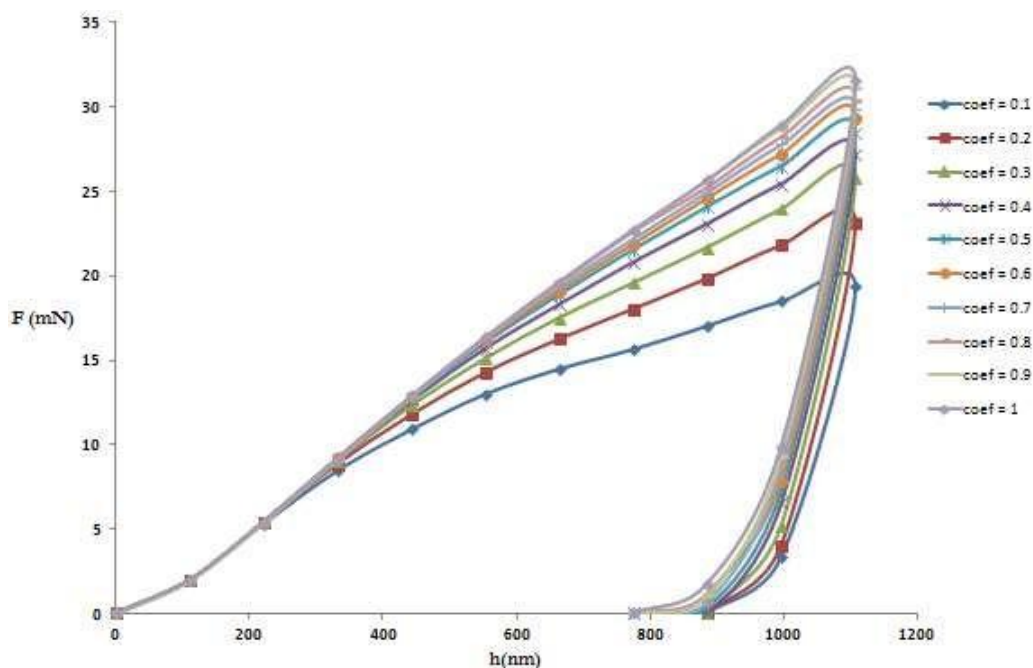


Figure 16: Evolution of the force-displacement curve for various values of the friction coefficient

### 5.3 Influence of parameters associated with mechanical behaviour

As seen above, the parameters linked to the mechanical behaviour model are 8 in number. Elastic characteristics and strengths are known to influence the force-depth simulation curve. This paragraph aims at identifying the parameters of the plastic behaviour with the most significant influence on the indentation behaviour. This can later allow the number of unknown variables to be reduced. Thus, a sensitivity analysis sequentially performed for each parameter is presented in this section. As for the sensitivity analysis on the friction coefficient, the starting set of the materials parameters is  $E=48$  GPa,  $\nu=0.32$ ,  $R_c=50$  MPa,  $R_t=3.6$  MPa,  $\Psi=35^\circ$ ,  $K=0.66$ ,  $\alpha=1.16$  and  $e=0$ .

#### 5.3.1 Sensitivity study on the dilation angle

The dilation angle is a major parameter which governs the Drucker-Prager plastic flow potential. This law makes it possible to quantify the plastic strain rate and therefore allows plastic strain to occur during loading. Figure 17 presents the results for different values of  $\psi$ . A significant influence of the dilation angle may be observed: it has an influence on mainly the maximum force, but also on the residual indentation depth after

unloading. On the other hand, it does not affect the unloading curve slope. The smaller the dilation angle, the greater the residual indentation depth.

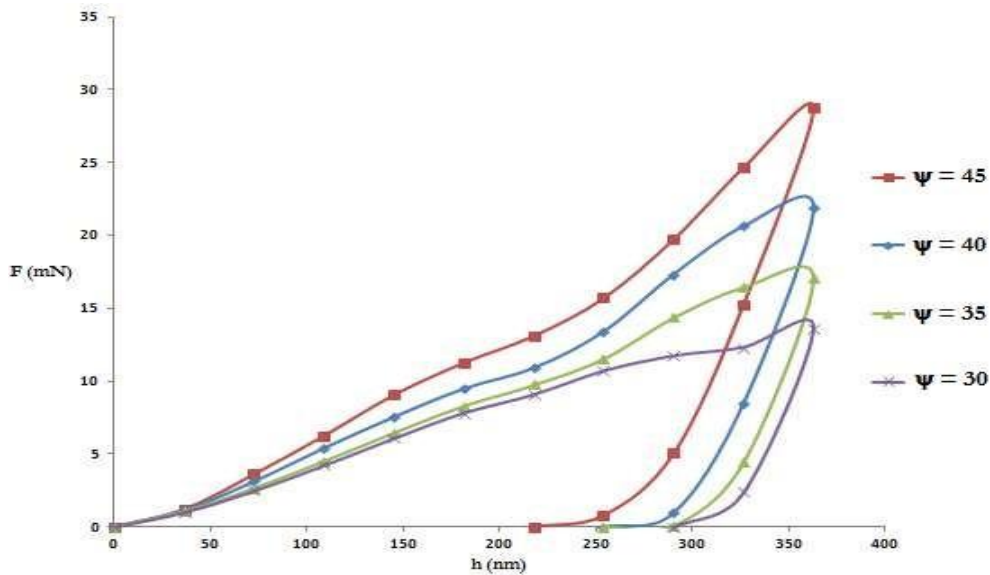


Figure 17: Evolution of the force-displacement curve for various values of the dilation angle  $\psi$

### 5.3.2 Sensitivity study on the eccentricity

Three values of the eccentricity, appearing in the hyperbolic shape of Drucker–Prager flow potential, are tested. Figure 18 shows a weak influence of this parameter. Later, the zero value will be kept by default.

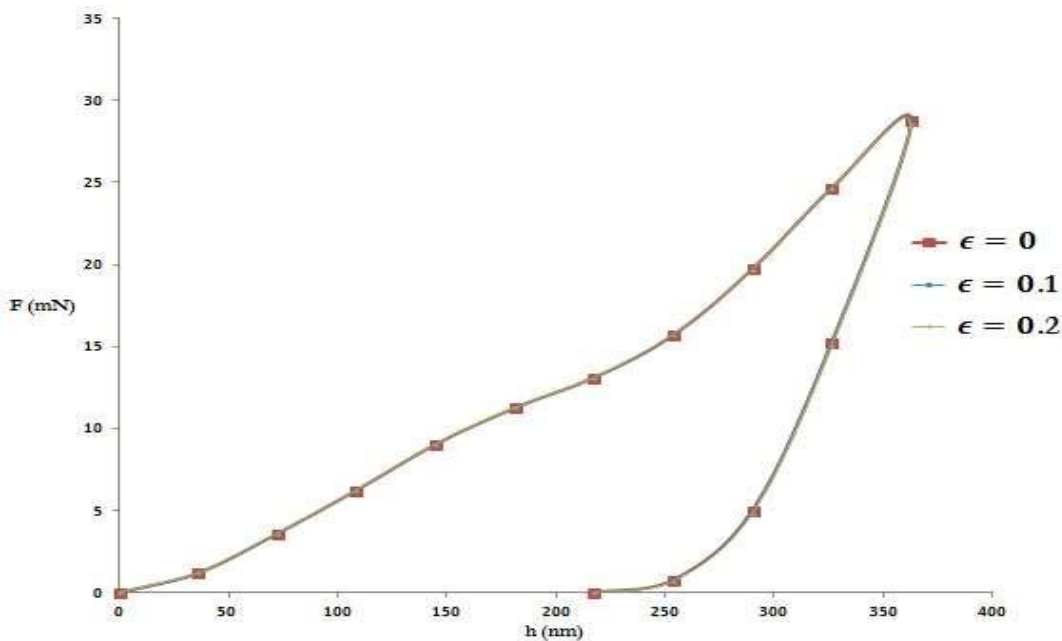


Figure 18: Evolution of the force displacement curve for various values of the eccentricity  $\epsilon$

### 5.3.3 Sensitivity study on the $f_b/f_{c0}$ ratio

Four values of the  $f_b/f_{c0}$  ratio are tested. Figure 19 shows the significant influence of this parameter on the results. It affects obviously the maximal force, and has also an influence on the residual indentation depth of the unloading curve. It is worth noting that this ratio modifies significantly the slope of the curve before the peak and a ratio lower than 1 does not enable one to obtain the experimentally observed stiffening. On the following,

this ratio will be considered to be higher than 1.1. On the other hand, the  $f_b/f_{co}$  ratio does not affect the initial unloading curve slope.

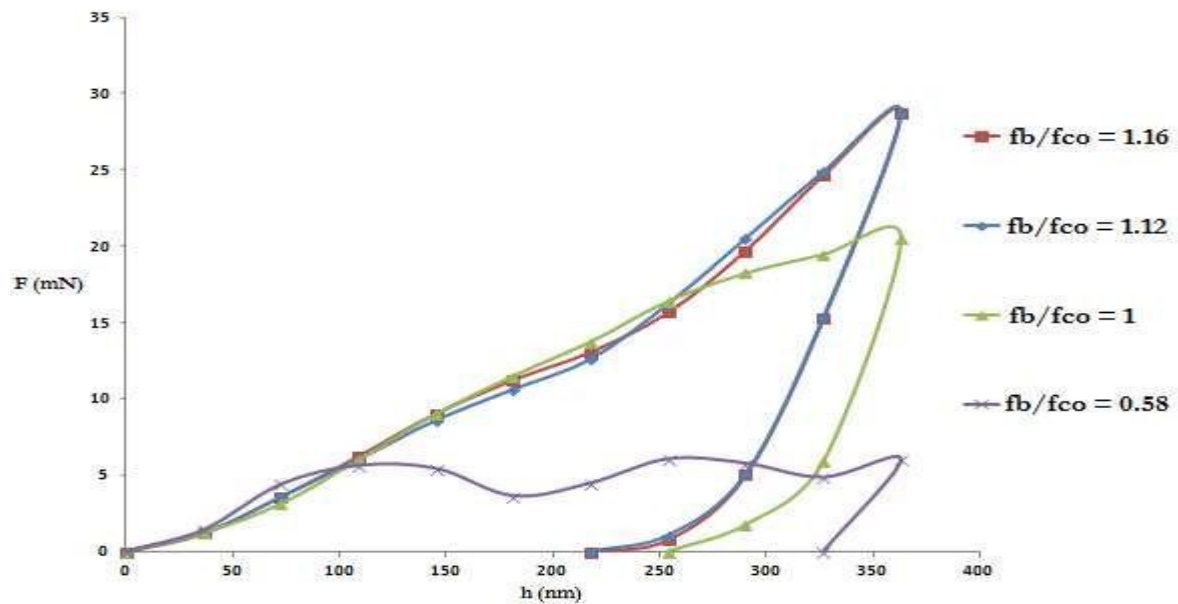


Figure 19: Evolution of the force-displacement curve for various values of the  $f_b/f_{co}$  ratio.

### 5.3.4 Sensitivity study on the K-parameter

Parameter K is one of the important parameters of the model. It represents the ratio of the second stress invariant on the tensile meridian to that of the compressive meridian. K is directly related to the internal friction angle [63]. It controls the material deformation capacity in Lubliner’s model. From the results of the sensitivity analysis presented in Figure 20, it appears that the greater K and the more it tends to the more deformable the material can become. On the other hand, if K tends to 0.5, the material becomes less deformable. The residual displacement and the hysteresis of the force-depth curve decreases.

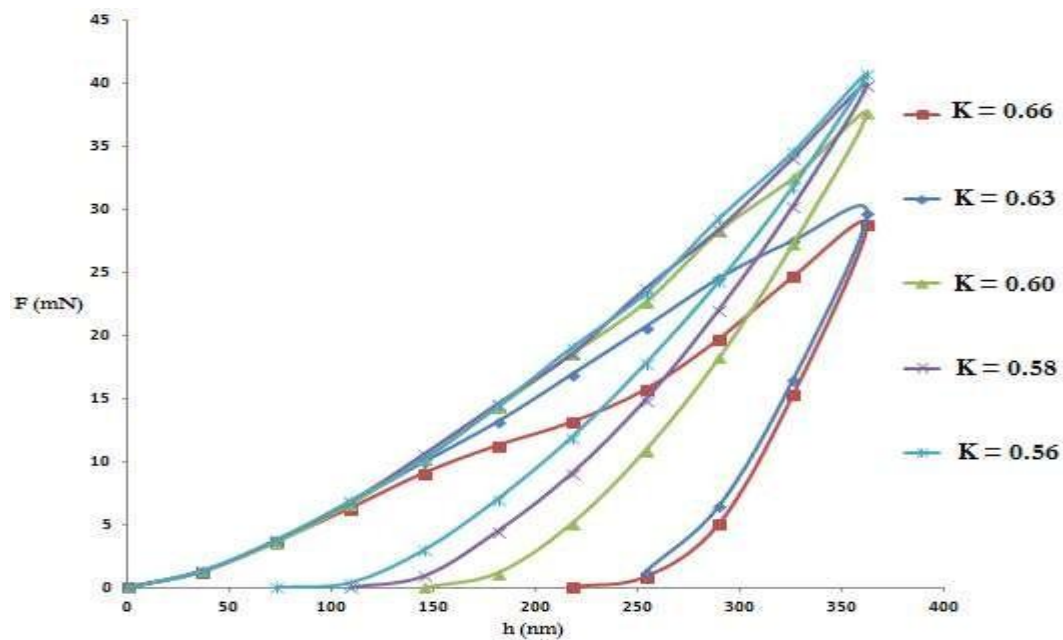


Figure 20: Evolution of the force-displacement curve for various values of K-parameter

### 5.3.5 Summary of the main results of the sensitivity analysis

To summarize the sensitivity analyses, the most influent parameters are the dilation angle  $\psi$ , the  $K$  parameter and the  $f_b/f_{co}$  ratio. The eccentricity does not affect the force-indentation depth simulation curve. Consequently, only those parameters are retained as variables for the various studied phases. The zero-value of the eccentricity is retained in the following, that enables one to reduce the number of parameters to identify.

## 5.4 Inverse analysis for the identification of the parameters associated with the mechanical behaviour model

### 5.4.1 Strategy

Even if the previous sensitivity analysis has put into evidence a non-influent parameter and thus has enabled one to reduce to 7 the number of unknown parameters to identify, this number is still important. However, the range of variation of each parameter is not totally unknown and some initial values may be suggested to simplify the inverse analysis procedure.

Once these initial values are introduced in the first step of the computation, the FE simulation may provide a first numerical response and an indentation force-depth curve. Starting from the discrepancy between simulated and experimental curves evaluated by the least-squares method for example, a new set of parameters is chosen and introduced in function of the conclusions of the sensitivity analysis. Then new simulation answers and discrepancy are obtained until, by iteration, the numerical curve is close enough to the experimental one. The 7 parameters associated with each phase behaviour law are then identified.

More precisely, the initial values choice and the identification process are carried as follows:

- choosing Young's modulus  $E$  and Poisson's coefficient  $\nu$  values. The choice is made so as to well reproduce the unloading part of the curve (see section 2);
- the  $f_b/f_{co}$  ratio value is set at 1.16 (value by default for concrete, assuming the ratio is shared by all the material components);
- the tensile strength is first supposed to be equal to  $E/10^4$  [16]. The resistance to compression is then fixed at  $R_c = 10 \cdot E/10^4$ , that is  $R_c = E/10^3$  (ten times the tensile strength);
- the dilation angle value is initially fixed at  $\psi = 35^\circ$ ;
- $K$  has an influence on the part of the curve before the peak, the maximum force value, and it is the only parameter of the plastic behaviour that has an influence on the unloading curve slope. Besides, it is known that  $K$  close to 0.5 is equivalent to a rigid material and  $K$  close to 1 is equivalent to a very deformable material. The value of  $K$  is identified on the unloading slope (and so without considering the part of the curve before the peak).  $K = 0.7$  may be chosen as a first value and the sensitivity study starts from this value.
- Once  $K$  is identified, the dilation angle value needed to correctly simulate the part of the curve before the peak is adjusted.
- If the two parameters,  $K$  and  $\psi$ , are no longer correlated, there is no need then to come back to the adjustment of  $K$  (and the post peak will not at all be influenced by the change in value of  $\psi$ ); otherwise it would be necessary to some come back to  $K$  and slightly readjust its value, then to  $\psi$ , etc;
- If the modeling – experiment discrepancy is not small enough, then it becomes necessary to go back to the beginning of the procedure and readjust the initial values.

### 5.4.2 Results: identification of parameters and comparison between experimental and simulation curves

The inverse method described above is applied on each phase of the matrix namely what was previously called: LD C-S-H, HD C-S-H, portlandite CH, sand and unhydrated clinker particles. After several loops in the iterative procedure, the mechanical behaviour parameters presented in Table 1 are obtained. This iterative procedure has finally found that the  $f_b/f_{co}$  ratio does not need to be readjusted from its initial value ( $f_b/f_{co}=1.16$ ).



**Table 1:** Parameters identified after applying the inverse iterative method. The  $f_b/f_{co}$  ratio is remained equal to 1.16

	LD C-S-H	HD C-S-H	CH	Sand	Unhydrated Clinker particles
Enum	18	25	40	63	90
$\nu$	0.24	0.25	0.345	0.35	0.27
$R_c$	27	40	46	79.51	111.66
$R_t$	1.49	3.24	3.509	5.168	6.628
$\psi$	35	40	40	43	43
K	0.66	0.66	0.62	0.5	0.5

Furthermore, Figures 21 to 25 present the comparisons between representative experimental curves and simulated ones obtained with the best fitted parameters of the mechanical behaviour model. A very good agreement is put into evidence, for both loading and unloading stage.

From Group1 to Group5, it can be noted that Young’s modulus  $E$ , compressive and tensile strengths  $R_c$  and  $R_t$  and dilation angle  $\psi$  increase while coefficient  $K$  decreases. The slight discrepancy in the results can be linked to various parameters such as the friction coefficient, which is difficult to determine, the plastic behaviour model choice, the identification procedure for the different phases.

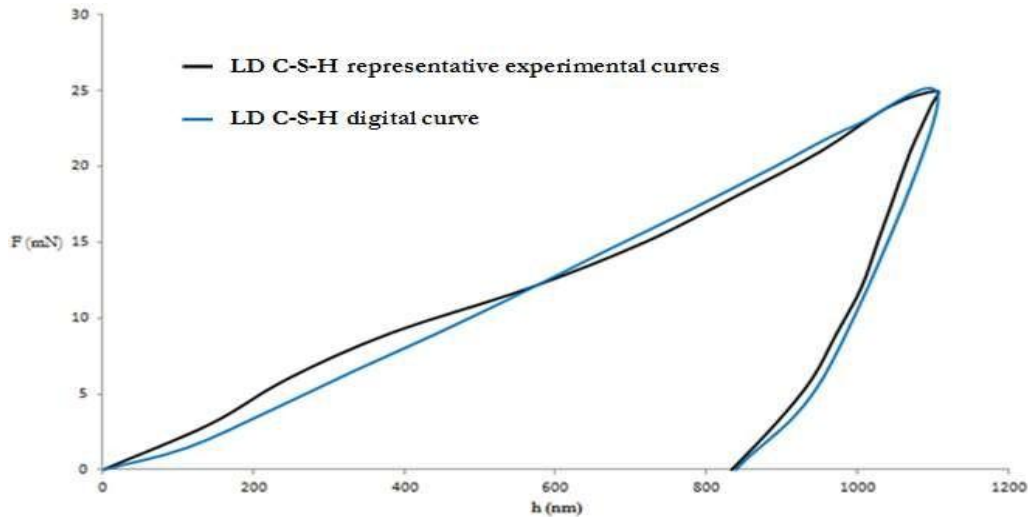


Figure 21: Results for LD C-S-H phase. Experimental and simulated curves after parametric identification

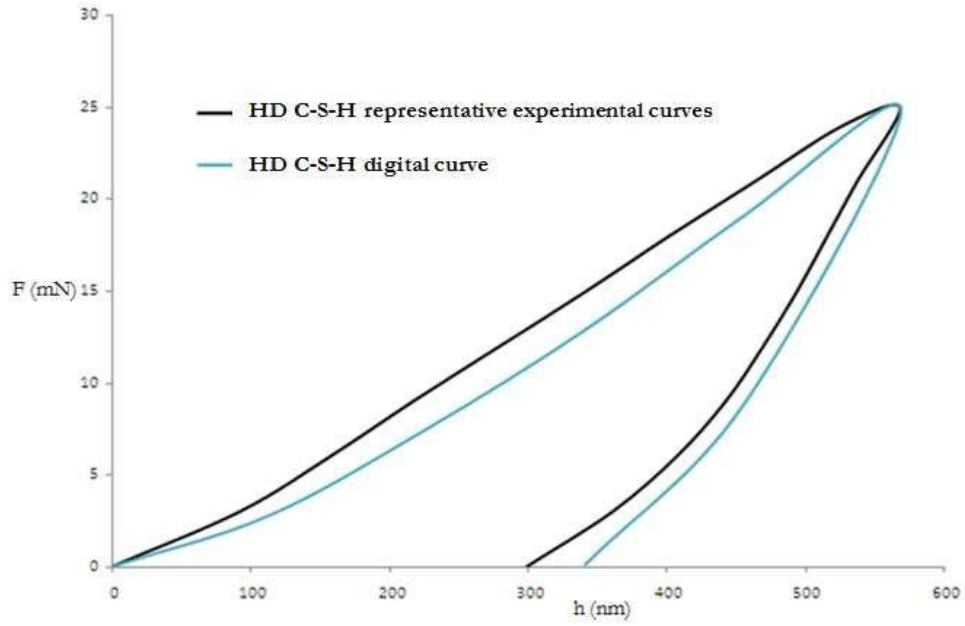


Figure 22: Results for HD C-S-H phase. Experimental and simulated curves after parametric identification

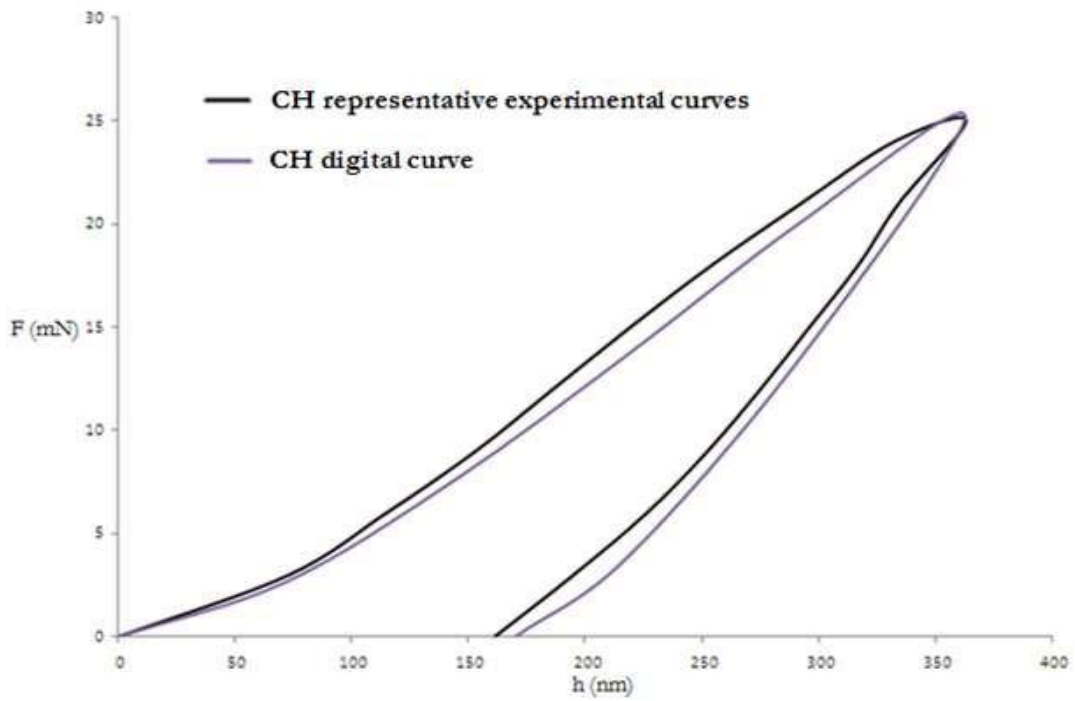


Figure 23: Results for Portlandite CH phase. Experimental and simulated curves after parametric identification

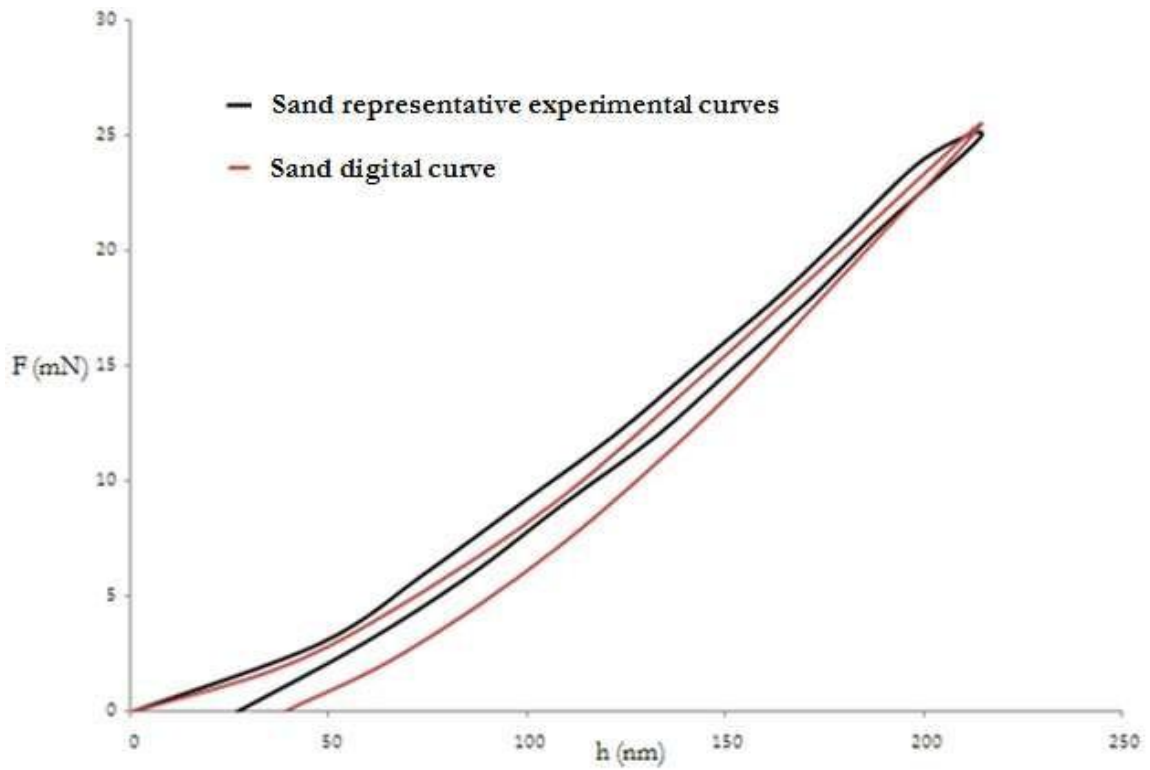


Figure 24: Results for Sand particles. Experimental and simulated curves after parametric identification

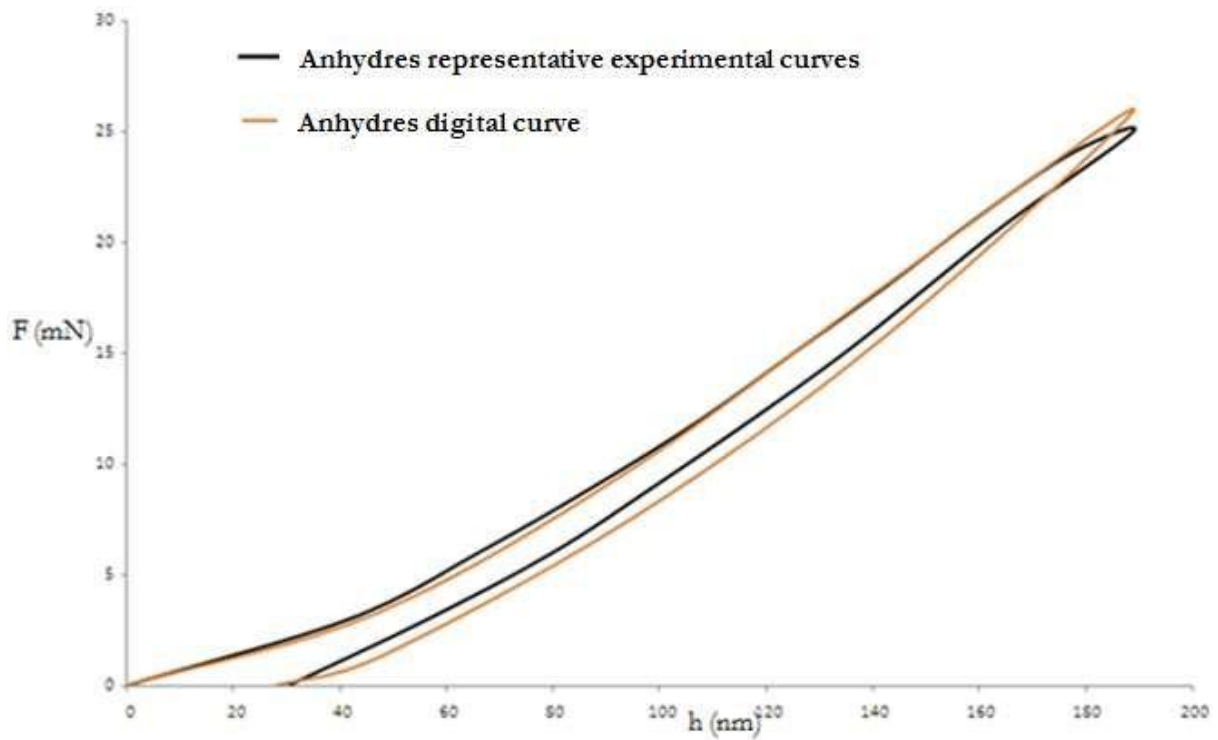


Figure 25: Results for unhydrated phases. Experimental and simulated curves after parametric identification

## 6. Conclusion

This paper presents first a micro-indentation experimental campaign conducted on a cementitious material. The particularity of this new study is that micro-indentation tests are performed on cement composite materials

(concrete) with sand particles and aggregates. The proportion of the various phases are thus those of the core of a real cementitious matrix and a possible modification due to the presence of aggregates is taken into account. Applying the indentation technique combined with SEM observations and micro-analysis has made it possible to identify the various phases of the cement matrix and their relative proportions as well as parameters linked to the mechanical behaviour such as the reduced elastic modulus and the hardness. A Finite Element simulation has been then developed and used in an inverse analysis procedure to assess the parameters of the elastic behaviour as well as, for the first time, those of a non-associated plasticity model. These results may be of interest all researchers working on the multi-scale modeling of cementitious material.

## References

- [1]. C. Zhang, W. Zhou, G. Ma, C. Hu and S. Li, A meso-scale approach to modeling thermal cracking of concrete induced by water-cooling pipes, *Computers and Concrete* 15 (4) (2015)
- [2]. J.J.C. Pituba, E.A. Souza Neto, Modeling of unilateral effect in brittle materials by a mesoscopic scale approach, *Computers and Concrete* 15 (5) (2015)
- [3]. Zhang, M., Jivkov, A.P., Micromechanical modelling of deformation and fracture of hydrating cement paste using X-ray computed tomography characterization, *Composites Part B: Engineering* 88 (2016) 64-72
- [4]. A. Gangnant, J. Saliba, C. La Borderie, S. Morel, Modeling of the quasibrittle fracture of concrete at meso-scale: Effect of classes of aggregates on global and local behavior, *Cement and Concrete Research* 89 (2016) 35-44
- [5]. J. Saliba, M. Matallah, A. Loukili, J.P. Regoin, D. Grégoire, L. Verdon, G. Pijaudier-Cabot, Experimental and numerical analysis of crack evolution in concrete through acoustic emission technique and mesoscale modelling, *Engineering Fracture Mechanics* 167 (2016) 123–137
- [6]. H. Zhang, B. Šavija, S.C. Figueiredo, E. Schlangen, Experimentally validated multi-scale modelling scheme of deformation and fracture of cement paste, *Cement and Concrete Research* 102 (2017) 175-186.
- [7]. V. Papadopoulos, M. Impraimakis, Multiscale modeling of carbon nanotube reinforced concrete, *Composite Structures* 182 (2017) 251-260
- [8]. N. Benkemoun, E. Roubin, J.-B. Colliat, FE design for the numerical modelling of failure induced by differential straining in meso-scale concrete: Algorithmic implementation based on operator split method, *Finite Elements in Analysis and Design* 137 (2017) 11-25
- [9]. A.I. Cuba Ramos, C. Roux-Langlois, C.F. Dunant, M. Corrado, J.-F. Molinari, HPC simulations of alkali-silica reaction-induced damage: Influence of alkali-silica gel properties, *Cement and Concrete Research* 109 (2018) 90-102
- [10]. J.-S. Lim, Y.-D. Jeong, S.-T. Yi, Size effect on compressive strength of concrete using meso-scale finite element method, *Journal of the Korea Concrete Institute* 30 (2018) 67-73
- [11]. A.B. Giorla, C.F. Dunant, Microstructural effects in the simulation of creep of concrete, *Cement and Concrete Research* 105 (2018) 44-53
- [12]. M. Farah, J. Saliba, F. Grondin, A. Loukili, Multi-Scale Methods for the Analysis of Creep-Damage Coupling in Concrete, in: *Advances in Multi-Physics and Multi-Scale Couplings in Geo-Environmental Mechanics* (2018) 205-241
- [13]. H. Zhang, B. Šavija, E. Schlangen, Towards understanding stochastic fracture performance of cement paste at micro length scale based on numerical simulation, *Construction and Building Materials* 183 (2018) 189-201
- [14]. T. Iskhakov, J.J. Timothy, G. Meschke, Expansion and deterioration of concrete due to ASR:
- [15]. Micromechanical modeling and analysis, *Cement and Concrete Research* Cement and Concrete Research 115 (2019) 507-518
- [16]. F. Bernachy-Barbe, B. Bary, Effect of aggregate shapes on local fields in 3D mesoscale simulations of the concrete creep behavior, *Finite Elements in Analysis and Design* 156 (2019) 13-23



- [17]. F. Bernard, S. Kamali-Bernard, W. Prince, 3D Multi-scale modelling of mechanical behaviour of sound and leached mortar, *Cement and Concrete Research* 38 (4) (2008) 449–458.
- [18]. I. Comby-Peyrot, F. Bernard, P.-O. Bouchard, F. Bay, E. Garcia-Diaz, Development and validation of a 3D computational tool to describe concrete behaviour at mesoscale. Application to the Alkali-Silica Reaction, *Computational Materials Science* 46 (2009) 1163–1177.
- [19]. S. Kamali-Bernard, F. Bernard, W. Prince, Computer modeling of tritiated water diffusion tests for cement-based materials, *Computational Materials Science* 45(2) (2009) 528–535.
- [20]. S. Kamali-Bernard, F. Bernard, Effect of tensile cracking on diffusivity of mortar: 3D numerical modelling, *Computational Materials Science* 47 (1) (2009) 178–185.
- [21]. F. Bernard, S. Kamali-Bernard, Performance simulation and quantitative analysis of cement-based materials subjected to leaching, *Computational Materials Science* 50 (1) (2010) 218-226.
- [22]. F. Bernard, S. Kamali-Bernard, Predicting the evolution of mechanical and diffusivity properties of cement pastes and mortars for various hydration degrees - A numerical simulation investigation, *Computational Materials Science* 61 (2012) 106-115.
- [23]. D. Keinde, S. Kamali-Bernard, F. Bernard, I.K. Cissé, Effect of the interfacial transition zone and the nature of the matrix-aggregate interface on the overall elastic and inelastic behaviour of concrete under compression: a 3D numerical study, *European Journal of Environmental and Civil Engineering* 18 (10) (2014) 1167-1176.
- [24]. F. Bernard, S. Kamali-Bernard, Numerical study of ITZ contribution on mechanical behavior and diffusivity of mortars, *Computational Materials Science* 102 (2015) 250-257.
- [25]. D. Niknezhad, B. Raghavan B., F. Bernard, S. Kamali-Bernard, Towards a realistic morphological model for the meso-scale mechanical and transport behavior of cementitious composites, *Composites Part B: Engineering* 81 (2015) 72-83.
- [26]. B. Raghavan, D. Niknezhad, F. Bernard, S. Kamali-Bernard, Combined meso-scale modeling and experimental investigation of the effect of mechanical damage on the transport properties of cementitious composites, *Journal of Physics and Chemistry of Solids* 96 (2016) 22-37.
- [27]. L. Sow, F. Bernard, S. Kamali-Bernard, C.M.F. Kébé, Mesoscale modeling of the temperaturedependent viscoelastic behavior of a Bitumen-Bound Gravels, *Coupled Systems Mechanics* 7 (5) (2018) 509-524.
- [28]. R.F. Feldman, C.Y. Huang, Properties of Portland cement-silica fume pastes: II. mechanical properties, *Cement and Concrete Research* 15 (1985) 943–952.
- [29]. S. Igarashi, A. Bentur, S. Mindess, Characterization of the microstructure and strength of cement paste by microhardness testing, *Advanced Cement Research* 8 (1996) 87–92.
- [30]. W. Zhu, P.J.M. Bartos, Assessment of interfacial microstructure and bond properties in aged (GRC) using a novel microindentation method, *Cement and Concrete Research* 27 (1997) 1701–1711.
- [31]. W. Zhu, P.J.M. Bartos, Application of depth-sensing microindentation testing to study of interracial transition zone in reinforced concrete, *Cement and Concrete Research* 30 (2000) 1299–1304.
- [32]. P. Trtik, C.M. Reeves, P.J.M. Bartos, Use of focused ion beam (FIB) for advanced interpretation of microindentation test results applied to cementitious composites, *Materials & Structures* 33 (2000) 189–193.
- [33]. G. Constantinides, F.-J. Ulm, K.J. Van Vliet, On the use of nanoindentation for cementitious materials, *Materials & Structures* 36 (2003) 191–196.
- [34]. G. Constantinides, F.-J. Ulm, The effect of two types of C-S-H on the elasticity of cement-based materials: results from nanoindentation and micromechanical modeling, *Cement and Concrete Research* 34 (2004) 67–80.
- [35]. K.L. Scrivener, P.L. Pratt, A Preliminary Study of the Micro-structure of Cement/Sand/Bond in Mortar, In: *Proceedings of 8th International Congress on the Chemistry of Cement*, Rio de Janeiro, Brazil (1986) 466-471.
- [36]. H.M. Jennings, A model for the microstructure of calcium silicate hydrate in cement paste. *Cement and Concrete Research* 30 (1) (2000) 101-116.



- [37]. M.J. De Jong, F.-J. Ulm, The nanogranular behavior of CSH at elevated temperature (up to 700° C), *Cement and Concrete Research* 37 (2007) 1-12.
- [38]. J. Fu, PhD thesis, National Institute of Applied Sciences – Rennes 2016
- [39]. J. Fu, F. Bernard, S. Kamali-Bernard, Assessment of the elastic properties of amorphous calcium silicates hydrates (I) and (II) structures by molecular dynamics simulation”, *Molecular Simulation*, 39(14-15) (2018) 1-15.
- [40]. L. Sorelli, G. Constantinides, F.J. Ulm, F. Toutlemonde, The nano-mechanical signature of ultra high performance concrete by statistical nanoindentation techniques, *Cement and Concrete Research* 38 (2008) 1447–1456.
- [41]. W.G. Li, J.Z. Xiao, Z.H. Sun, S. Kawashima, S.P. Shah, Interfacial transition zones in recycled aggregate concrete with different mixing approaches, *Construction and Building Materials* 35 (2012) 1045–1055.
- [42]. Trtik P, Münch B, Lura P. A critical examination of statistical nanoindentation on model materials and hardened cement pastes based on virtual experiments, *Cement and Concrete Composites* 31 (2009) 31 705–714.
- [43]. F.-J. Ulm, M. Vandamme, H.M. Jennings, J. Vanzo, M. Bentivegna, K.J. Krakowiak, G. Constantinides, C.P. Bobko, K.J. Van Vliet, Does microstructure matter for statistical nanoindentation techniques?, *Cement and Concrete Composites* 32 (1) (2010) 92-99.
- [44]. P. Lura, P. Trtik, B. Münch, Validity of recent approaches for statistical nanoindentation of cement pastes, *Cement & Concrete Composites* 33 (2011) 457–465.
- [45]. H. Liu, X. Ren, J. Li, Indentation tests based multi-scale random media modeling of concrete, *Construction and Building Materials* 168 (2018) 209–220
- [46]. M. Vandamme, F. -J. Ulm, Nanoindentation investigation of creep properties of calcium silicate hydrates, *Cement and Concrete Research* 52 (2013) 38-52.
- [47]. L. Zhang, M. Mahdi, The plastic behaviour of silicon subjected to micro-indentation, *Journal of Materials Science* 31 (21) (1996) 5671–5676
- [48]. A. Muchtar, L. C. Lim, K. H. Lee, Finite element analysis of vickers indentation cracking processes in brittle solids using elements exhibiting cohesive post-failure behavior, *Journal of Materials Science* 38 (2) (2003) 235-243.
- [49]. A.K. Reinhardt, M. Sheyka, M. Tehrani, M. Al - Haik, M. M. Reda Taha, Experimental and Numerical Investigation of Nanoindentation of Self-Consolidating Concrete, *Proceedings of the Society for Experimental Mechanics Annual Conference*, Albuquerque, New Mexico, USA, June 1-4, 2009.
- [50]. L.Meng, P.Breitkopf, B.Raghavan, G.Mauvoisin, O.Bartier, X.Hernot, Identification of material properties using indentation test and shape manifold learning approach, *Computer Methods in Applied Mechanics and Engineering* 297 (2015) 239-257.
- [51]. L. Meng, P. Breitkopf, G. Le Quilliec, An insight into the identifiability of material properties by instrumented indentation test using manifold approach based on P-h curve and imprint shape, *International Journal of Solids and Structures* 106–107 (2017) 13-26.
- [52]. L. Meng, B. Raghavan, O. Bartier, X. Hernot, G. Mauvoisin, P. Breitkopf, An objective metamodeling approach for indentation-based material characterization, *Mechanics of Materials* 107 (2017) 31-44.
- [53]. E. Hervé, S. Caré, J.P. Seguin, Influence of the porosity gradient in cement paste matrix on themechanical behavior of mortar, *Cement and Concrete Research* 40 (7) (2010) 1060-1071.
- [54]. K. Velez, S. Maximilien, D. Damidot, G. Fantozzi, F. Sorrentino. Determination by nanoindentation of elastic modulus and hardness of pure constituents of porland cement clinker. *Cement and Concrete Research* 31 (2001) 555-561.
- [55]. W.C. Oliver, G.M. Pharr GM, Improved technique for determining hardness and elastic modulus using load and displacement sensing indentation experiments, *Journal of Material Research* 7 (6) (1992) 1564–1583.
- [56]. J. Monge, Fissuration des mortiers en couches minces-Effets de l’hydratation, du séchage et de la carbonatation. PhD thesis, ENS Cachan (2007) in French



- [57]. S. Ghabezloo, Association of macroscopic laboratory testing and micromechanics modeling for the evaluation of the poroelastic parameters of a hardened cement paste. *Cement and Concrete Research* 40 (2010) 1197-1210.
- [58]. H.M. Jennings, Colloid model of C–S–H and implications to the problem of creep and shrinkage, *Materials and Structures* 37 (1) (2004) 59–70.
- [59]. J. Lubliner, J. Oliver, S. Oller, E.A. Onate, A plastic-damage model for concrete. *International Journal of Solids and Structures* 25 (1989) 299-329.
- [60]. J. Lee, G.L. Fenves, Plastic-Damage Model for Cyclic Loading of Concrete Structures. *Journal of Engineering Mechanics* 124 (8) (1998) 892–900.
- [61]. ABAQUS, Abaqus User's manual. ABAQUS Inc./ Simulia (2018)
- [62]. T. Jankowiak, P.T. Łodygowski, Identification of parameters of concrete damage plasticity consecutive model. *Foundations of civil and environment engineering* 6 (2005) 53-69.
- [63]. E. Sarris, G. Constantinides, Finite element modeling of nanoindentation on C–S–H: effect of pileup and contact friction, *Cement and Concrete Composites* 36 (2013) 78–84.
- [64]. L. Sow, Approach coupled with experimentation - multi-scale modeling to determine the mechanical behavior of gravel roads treated with binders. Application to the recovery of bottom ash from non-hazardous waste incineration., PhD thesis, INSA Rennes (2018) in French.

